# Numerical simulation of air flow field in single-sided ventilated buildings

K.A. Papakonstantinou, C.T. Kiranoudis*, N.C. Markatos

*Department of Chemical Engineering, National Technical University of Athens, Zographou Campus, Athens 15 780, Greece*

## Abstract

The present paper refers to the numerical prediction of air velocities and temperatures inside single-sided naturally ventilated buildings and more specifically the special case in which air from the external environment is brought into the building through single-directed openings.

The work is focused on the physical procedures governing air movement during the single-sided natural ventilation. The study presents a mathematical model, implemented in a general computer code, that can provide detailed information on velocity and temperature, prevailing in three-dimensional, single-sided ventilated buildings with openings of any geometrical complexity, for given external meteorological conditions. The mathematical model involves the partial differential equations governing flow and heat transfer in large enclosures. Turbulent flow is simulated and buoyancy effects are taken into account. The model is used to assess the environmental conditions in a test cell designed and constructed by the National Observatory of Athens with external conditions corresponding to their measurements. The numerical results are in good agreement with the experimental values of air velocity, temperature and pressure, at various sites inside the test cell. © 2000 Elsevier Science S.A. All rights reserved.

## 1. Introduction

The ventilation of internal spaces, that is the refreshment of closed spaces, constitutes unquestionably one of the fundamental requirements for the achievement of appropriate conditions of healthy and thermally comfortable buildings, without creating significant wind currents that may disturb or create noise. The term 'ventilation' includes all thermal procedures where air in the interior of a closed space is replaced by external air masses, entering through building openings. The natural ventilation contributes to the improvement of thermal comfort and quality conditions of the internal air, while at the same time it is recognised as a very efficient technique that, when applied properly, leads to a significant reduction of energy consumption for the cooling of buildings. The combination of the above characteristics establishes natural ventilation as the best solution, especially for areas where the prevailing climatic conditions favour its implementation.

Natural ventilation thermal effects depend on air temperature and air flow velocity in the interior of residential spaces. More specifically, airflow velocity is the most important factor of assessing thermal feeling during ventilation, because it relieves the 'hot' and 'humid' feeling even if air temperature remains constant. Furthermore, air temperature is influenced by various indistinguishable factors that make it almost impossible to control air temperature without air conditioning devices. On the other hand, it may be possible to influence indoor airflow distribution by adjusting the size and position of openings and the shape of rooms, for given outdoor wind conditions. As a consequence, it is particularly useful to predict the air flow distribution in a building by natural ventilation and to design the entire building layout in order to utilise the natural cooling resources.

There are two popular methods to predict airflow fields; the first is the model experiment, and the second is the numerical simulation. The latter has a lot of advantages, for example flexibility in shaping the house layout and in setting the exact parameters of airflow, if appropriate mathematical models and efficient computer codes are available. Furthermore, computer costs decrease continuously, while labour and materials costs rise.

The advantages in using numerical methods to analyse ventilation performance have been pointed out by Murakami [1] and Liddament [2]. In particular, Liddament [2] concluded that the predictions obtained by numerical methods have enabled the concepts of ventilation efficiency to be applied at the design stage, while the value of the experi-

* Corresponding author. Tel.: +30-1-772-1503; fax: +30-1-772-3228.
*E-mail address:* kyr@chemeng.ntua.gr (C.T. Kiranoudis).

**Nomenclature**

| | |
|---|---|
| $A_n$ | convection-diffusion coefficient |
| $C$ | coefficient of $\varphi$ |
| $G$ | turbulence production rate |
| $h$ | enthalpy (J kg$^{-1}$) |
| $k$ | kinetic energy of turbulence (J kg$^{-1}$) |
| $P$ | pressure (Pa) |
| $R$ | gas constant (J mol$^{-1}$ K$^{-1}$) |
| $S_\varphi$ | source rate per unit volume |
| $T$ | temperature (K) |
| $\vec{u}$ | velocity vector components (m s$^{-1}$) |
| $V$ | value of $\varphi$ |

*Greek symbols*

| | |
|---|---|
| $\Gamma_\varphi$ | effective exchange coefficient of $\varphi$ |
| $\varepsilon$ | eddy dissipation rate (J s$^{-1}$ kg$^{-1}$) |
| $\mu$ | viscosity (kg m$^{-1}$ s$^{-1}$) |
| $\rho$ | density (kg m$^{-3}$) |
| $\sigma$ | Prandtl number for variable $\varphi$ |
| $\varphi$ | the general dependent variable |
| $\varphi_P$ | the general dependent variable at point P (centre of the control volume) |

mental method has been restricted to the evaluation and diagnostic studies on existing structures. In numerical methods, a flow system, as the one considered here, is divided into a grid of cells. A system of conservation equations is then solved for each cell, after specifying boundary conditions for the domain of interest. The flow structure within the flow system is therefore simulated with the predicted spatial distribution of the air velocity.

The present paper refers to the study of fluid flow and heat and mass transport phenomena take place inside buildings. The developed procedure was applied, for validation purposes, to simulate the indoor condition, of an experimental chamber. This chamber was constructed on Penteli mountain by the National Observatory of Athens (NOA), for the purpose of a detailed study of 'single-sided natural ventilation'. In the experiments, a closed space communicates with the external environment through one or more openings, that in all cases have the same orientation [3]. The geometry of the chamber as well as the boundary conditions applied, are appropriately represented in the mathematical model. The computational procedure, adopted for the evaluation of such a three-dimensional turbulent flow, is based on the solution of the governing equations for the dependent variables, that is the three velocity components, the pressure and the temperature by means of the finite volume technique [4,5]. Air flow is considered, turbulent, steady, although the model can handle transient phenomena if necessary, and the effects of buoyancy are taken into account. Turbulent flow was described through the use of the widely used $k$-$\varepsilon$ turbulence model. All of the above are implemented through

the computational framework of PHOENICS, a computational fluid dynamic (CFD) commercial code [6].

Different cases were examined concerning the geometry of chamber's openings as well as the external environmental conditions, aiming at the validation and examination of the performance of the mathematical model under different meteorological conditions as well as human interventions. The numerical simulation results are compared with the experimental measurements of velocity, pressure and temperature, measured at various sites inside the experimental chamber.

## 2. Mathematical formulation and application of the model

### 2.1. The differential equations

For steady-state flow, conservation equations for momentum, mass and energy can be expressed by means of the following general equation for the general dependent variable $\varphi$ [6]:

$$\frac{\partial}{\partial x_i}(\rho u_i \varphi) = \frac{\partial}{\partial x_i}\left(\Gamma_\varphi \frac{\partial \varphi}{\partial x_i}\right) + S_\varphi \tag{1}$$

where $\rho$ is the density, $S_\varphi$ the source/sink rate per unit volume for dependent variable $\varphi$ and $\Gamma_\varphi$ is the effective exchange coefficient of $\varphi$ [7]. The dependent variables of interest here are $u$, $v$, $w$, the three velocity components, $P$ the pressure, $T$ the temperature, $k$ the kinetic energy and $\varepsilon$ is the turbulence dissipation rate.

The source rate and the effective exchange coefficient corresponding to each variable $\varphi$ considered in this study are given in Table 1.

The values of constants $C_1$ and $C_2$ for the $k$-$\varepsilon$ turbulence model are 1.44 and 1.92, respectively [6]. The buoyancy sources are included in the appropriate momentum equation, as explained in [8–10].

### 2.2. The solution method

In order to solve the set of the above-mentioned seven differential equations, the finite-domain technique is used that combines features of the methods proposed by Patankar and Spalding [4], Spalding [5] and a whole-field pressure-correction solver [11]. The space dimensions were discretized into finite intervals and the variables were computed at a finite number of grid points. These variables are connected to each other through algebraic equations derived by integration of the differential equations over the control volumes defined by the above grid. This leads to algebraic equations of the form

$$\sum_n (A_n^\varphi + C)\varphi_P = \sum_n A_n^\varphi \varphi_n + CV \tag{2}$$

Table 1
Source rate and effective exchange coefficient for each $\varphi$

| Equation | $\varphi$ | $S_\varphi$ | $\Gamma_\varphi$ |
|---|---|---|---|
| Continuity | 1 | 0 | 0 |
| Momentum | $u_i$ | $-\dfrac{\partial p}{\partial x_i} + \left(\rho_{\text{ref}} - \dfrac{p}{RT}\right)g_i$ | $\mu$ |
| Energy | $h$ | 0 | $\dfrac{\mu}{\sigma_h}$ |
| Kinetic energy of turbulence | $k$ | $G - \rho\varepsilon$ | $\dfrac{\mu}{\sigma_k}$ |
| Eddy dissipation rate | $\varepsilon$ | $C_1\dfrac{\varepsilon}{k}G - C_2\rho\dfrac{\varepsilon^2}{k}$ | $\dfrac{\mu}{\sigma_\varepsilon}$ |
| The turbulence production rate | $G$ | $G = \mu_1\left(\dfrac{\partial u_i}{\partial x_j} + \dfrac{\partial u_j}{\partial x_i}\right)\dfrac{\partial u_i}{\partial x_j}$ | |

where the $\sum_n$ is over the cells adjacent to a defined point P. The coefficients $A_n^\varphi$, accounting for convective and diffusive fluxes across the elemental grid cells, are formulated using hybrid differencing [7]. The source terms can be written in the linear form

$$S_\varphi = C(V - \varphi) \tag{3}$$

where $C$ and $V$ stand for a coefficient and a value of the variable $\varphi$, respectively. Pressure values were obtained from a pressure-correction equation yielding the pressure change necessary to procure velocity changes that satisfy the mass continuity equation. To solve the three-dimensional flow equations, the SIMPLEST algorithm of Spalding is followed [4], in which finite-domain coefficients of the momentum equations contain only diffusion contributions, the convection terms being added to the linearised source term. The $w$-momentum equation was solved by a line-by-line procedure using the well-known TDMA method [12], while the $u$- and $v$-momentum equations were solved by a point-by-point procedure. The pressure-correction equation was solved over the whole-field [5]. The present model was implemented in the general computer program PHOENICS [6].
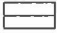
### 2.3. Test cases considered

The model was used to assess the indoor conditions in a test chamber designed and constructed by the NOA with external atmospheric conditions measured by the NOA group [3]. The geometry of the experimental chamber

and the conditions prevailing are given in Table 2, while in Fig. 1(a) the experimental chamber is presented. Concerning the opening sizing through which ventilation of the chamber was performed, three different cases are examined: wide-open, half-open and one-eighth-open window, all with two variations: with and without sun-shadings. Fig. 1(b) depicts schematically the window with sun-shadings. In particular, for the half-open window case the influence of the air velocity and temperature on the flow field inside the chamber was studied, by changing the inlet conditions. All of these cases demonstrate the ability of the present model to estimate accurately experimental measurements, according to the meteorological conditions and the geometry of the opening. The walls of the chamber as well as the sun shading of the opening were modelled by means of the 'porosity' concept [13]. According to this approach, each domain cell is characterised by a set of fractions. These fractions determine the proportion of the cell volume that is available for the fluid, and the proportion of each cell-face area available for flow, by convection and diffusion, from cell to its neighbour in a given direction. The program used calculates the flow and the temperature fields throughout the three-dimensional domain described above.

### 2.4. Boundary conditions

Boundary conditions are specified as follows. The inlet boundary was placed far enough from the experimental chamber so that conditions inside could not be influenced.

Table 2
Input data used in computations for NOA chamber[a] case

| Data | A | B | A | B | A | B |
|---|---|---|---|---|---|---|
| Outdoor air temperature (K) | 305.584 | 302.600 | 301.282 | 303.580 | 304.286 | 305.263 |
| Wall temperature (K) | 306.660 | 307.200 | 305.750 | 303.550 | 310.160 | 307.520 |
| Outdoor air velocity (m s$^{-1}$) | 0.3596 | 4.138, 10, 15 | 0.8165 | 0.4042 | 0.6620 | 1.3596 |

[a] A: with sun-shadings; B: without sun-shadings; chamber geometry $(x, y, z) = 2.76\ \text{m} \times 2.75\ \text{m} \times 5\ \text{m}$; air density $= 1.189\ \text{kg m}^{-3}$; air viscosity $= 10^{-5}\ \text{kg m}^{-1}\ \text{s}^{-1}$.
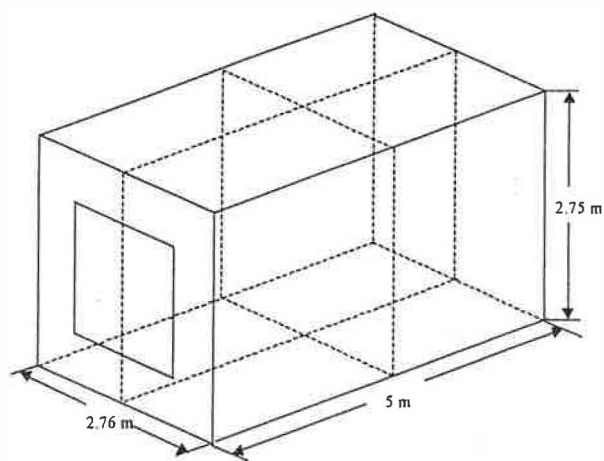
( a )
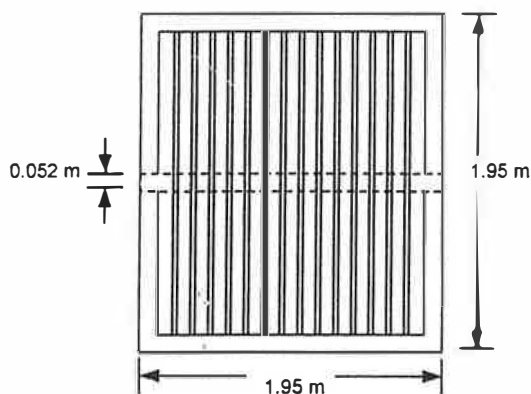


( b )
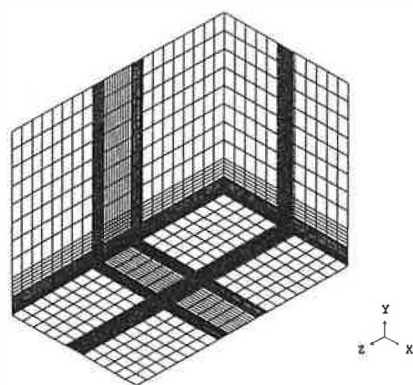


( c )

Fig. 1. (a) Experimental chamber; (b) window opening with sun-shadings and (c) a $36 \times 25 \times 49$ cells grid.

Known atmospheric flow and temperature conditions were fixed there. At chamber walls, velocities are set to zero and wall functions are used to calculate the wall shear stress [6]. Chamber walls were assumed isothermal.

### 2.5. Grid dependency and computer storage

The reported results have been obtained using a non-uniform grid consisting initially of 61 cells in the $x$-direction, 16 cells in the $y$-direction and 18 cells in the $z$-direction (17.568) for the case with sun-shadings. Then a $69 \times 25 \times 49$ cells (84 525 cells) grid was used, whose solutions are grid independent, as proved by repeating the run with even more cells. The computational grid used, initially, for the case without sun-shadings consisted of 25 cells in the $x$-direction, 16 cells in the $y$-direction and 24 cells in the $z$-direction (9600 cells) and then a $36 \times 25 \times 49$ cells (44 100 cells) grid was used, whose solutions are grid independent.

The calculations were performed on an $O_2$ Workstation (Silicon Graphics), with a CPU R 10000 processor and main memory of 64 MB.

### 2.6. Convergence and time requirements

A converged solution was defined as one that met the following criterion for all dependent variables:

$$\max|\varphi^{n+1} - \varphi^n| \leq 10^{-3} \tag{4}$$

between successive $n$ and $n+1$ sweeps of the iterative solution procedure. To improve convergence, under-relaxation was used. Relaxation of the 'false transient' type [12] was used for the three velocity components and for enthalpy. The value of the 'false time step' was 0.5 for the three velocity components and 0.001 for the enthalpy. For pressure, 'linear' relaxation of 0.1 was used. A typical CPU time for a run with the grid of 84 525 cells was 23.15 h and for the grid of 44 100 cells was 12.67 h, for full convergence.

## 3. Results and discussion

Space restrictions dictate that only some indicative results may be given in Table 3 as well as in Figs. 2–6. In Table 3 the

Table 3
Experimental and numerical temperature values of NOA chamber — half opening with sun-shadings

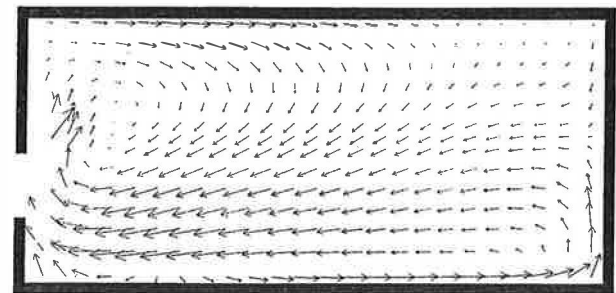| Coordinates of measurements' points | | | Experimental values | Numerical values |
|---|---|---|---|---|
| $x$ | $y$ | $z$ | | |
| 11.652 | 0.150 | 17.75 | 305.9 | 305.5 |
| 11.652 | 2.582 | 17.75 | 306.6 | 305.8 |
| 10.400 | 1.366 | 17.75 | 306.5 | 305.4 |
| 12.654 | 1.366 | 17.75 | 306.6 | 305.7 |
| 11.652 | 1.366 | 17.75 | 306.4 | 305.2 |
| 11.652 | 1.366 | 15.85 | 306.4 | 305.2 |
| 11.652 | 1.366 | 19.65 | 307.1 | 306.1 |
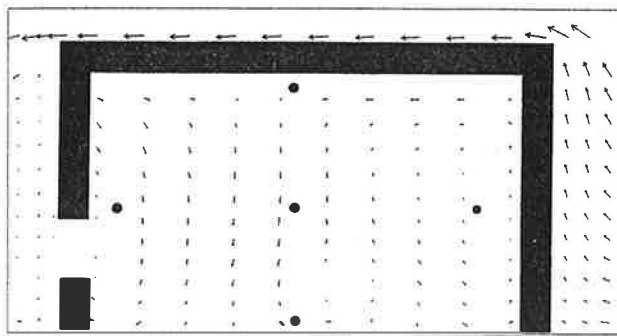
→ 0.15 m/s

( a )
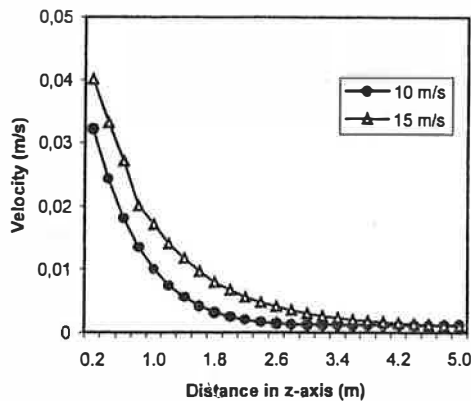


( b )

Fig. 2. (a) Velocity field of the z–y plane for the case of half-window-open with sun-shadings and (b) effect of air velocity on the flow field.



→ 0.04

(a)



→ 0.04

(b)

Fig. 3. Velocity fields of the z–y plane for the cases: (a) half-opening open without sun-shadings and (b) one-eighth-opening open without sun-shadings.

comparison between the experimental data and the numerical results is given. In Fig. 2(a) the velocity field on a z–y plane at $x=2.5$ m for the case of the half opening with sun-shadings is presented. In Fig. 2(b) the air velocity distribution is given. In Fig. 3 velocity fields for the cases of the half-open window and the one-eighth-open window (without sun-shadings), are presented again in the z–y plane at $x=2.5$ m. In Fig. 4 the effect of opening geometry is presented. In Fig. 5 the velocity fields of the whole opening being open, versus height of the experimental chamber is presented. Finally in Fig. 6 the temperature distribution of the half of the opening (without sun-shadings) is given in the y–z and y–x plane.
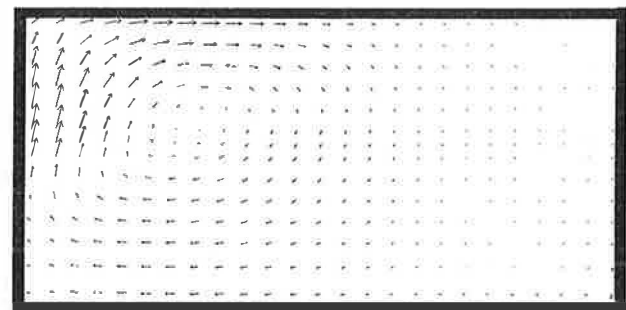
The comparison between the experimental data and the results calculated by the use of the computer code, is given in Table 3, for the case where air penetrates in the experimental chamber through the half opening (with sun-shadings). It can be seen that the predicted temperatures are lower than those measured experimentally, but they follow the same distribution.

The velocity field of the z–y plane for the case of the half opening with sun-shadings is presented in Fig. 2(a). As

indicated, two swirling motions are created inside the experimental room.

The velocity distribution at the middle plane is given in Fig. 2(b), at 1.381 m height from the chamber floor, through the whole length of the room (z-axis distance is measured starting from the opening). The results presented concern the case of the half-open window, without sun-shadings, and for two different inlet velocity values, 10 and 15 m s$^{-1}$. As presented, inflow of the air stream in the chamber causes a sharp reduction of velocity, while from the centre of the experimental chamber and along the room, outdoor air velocity do not have an important effect in the velocity flow field.

The velocity fields for the cases of the half-open and the one-eighth-open opening (without sun-shadings) in Fig. 3, are presented in the z–y plane, and more specifically at the middle plane and at 1.381 m height distance above ground. Two different geometries of the opening are examined: the half-open-opening and the one-eighth of it, through which air penetrates into the room. No sun-shadings are used. As seen in Fig. 1, where velocity field of the half-open-opening is presented, the velocity vectors have a higher value than those of the second figure, that one of the one-eighth-open of the opening. A swirl is been created just after the entrance of the chamber while in the opposite side of the chamber two
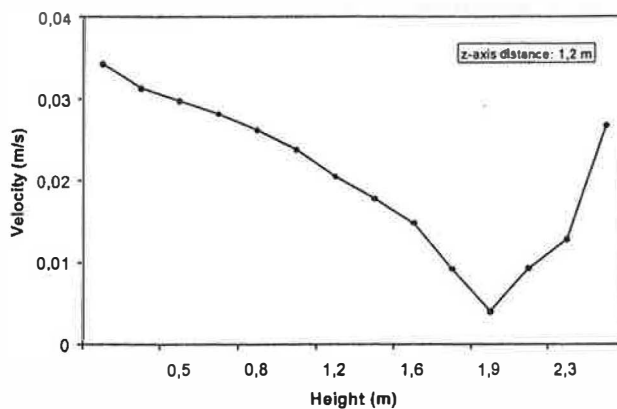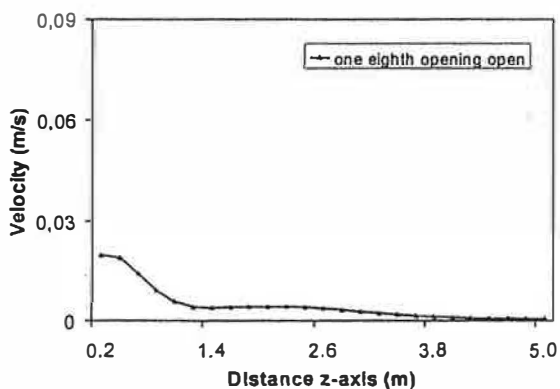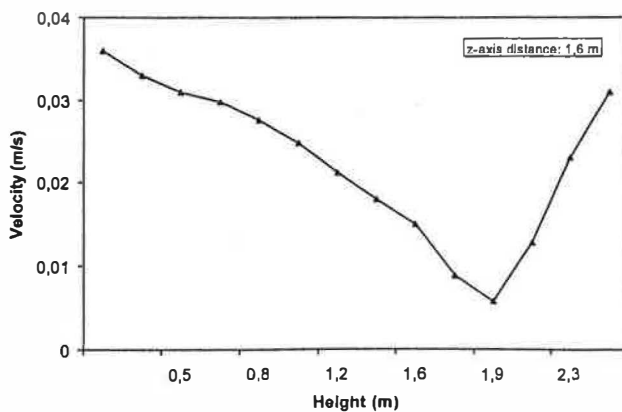
(a)



(b)
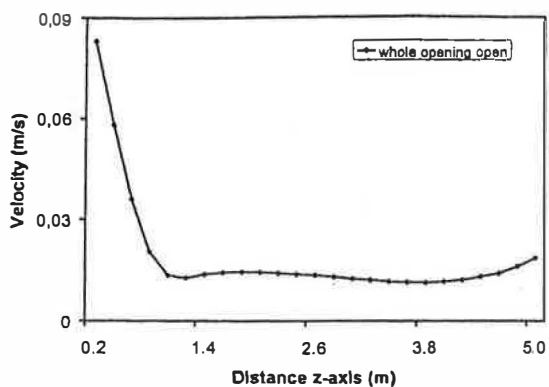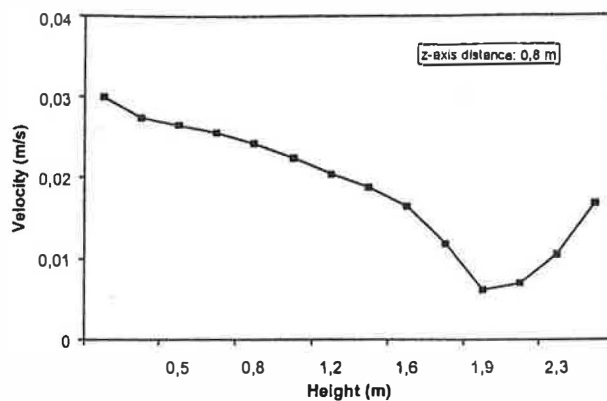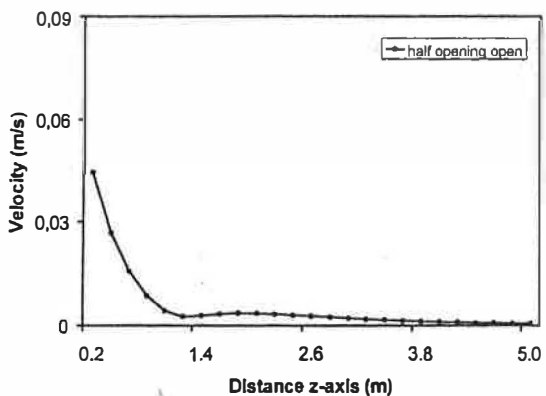


(c)

Fig. 4. Effect of the geometry of the opening on the flow field.



(a)



(b)



(c)

Fig. 5. Velocity field of the middle plane versus height of the chamber for the case of whole opening with sun-shadings: (a) $z$-axis distance: 0.8 m; (b) $z$-axis distance: 1.2 m and (c) $z$-axis distance: 1.6 m.

smaller swirls are been created. In the lower half plane of the room, air velocity has a greater value than that at the upper half. In Fig. 2, the magnitude of the velocity vectors is significantly smaller than the previous ones. A swirl is observed in the interior of the room, near the centre, while air velocity has very small values beyond the centre of the room (distance is measured starting from the opening).

The effect of chamber geometry of the opening is presented in Fig. 4. As presented in Fig. 3, velocity distribution inside the chamber is examined, for the same $z$–$y$ plane and in the middle of the room. As presented in this diagram the geometry of the opening influences the magnitude of the
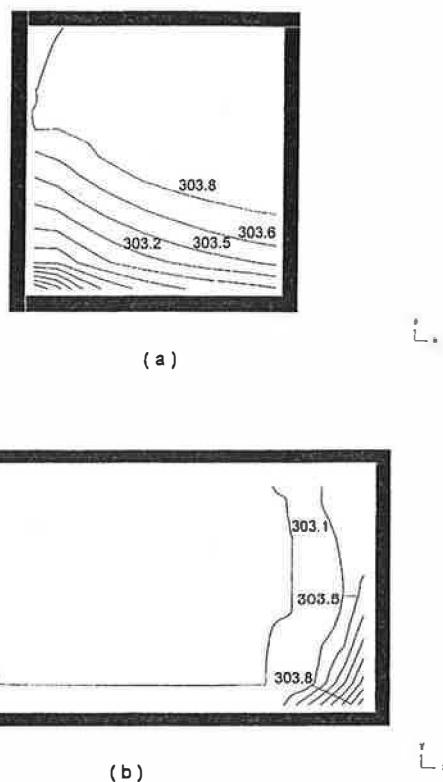
(a)



(b)

Fig. 6. Temperature distribution in the chamber for the case of the half-opening open with sun-shadings at z-axis distance 4.7 m: (a) y–x plane and (b) y–z plane.

velocity vectors for the first one-fifth of the room. Subsequently, the velocity values decrease rapidly.

The velocity field versus height of the experimental chamber is presented in Fig. 5, at the middle plane of the room for the case of the whole opening being open. Three different x–y planes of the room are presented: at $z=0.8$, 1.2 and 1.6 m. As indicated in Fig. 5, air velocity decreases as a function of room height by approximately a factor of two, until the height value of 2 m is reached. Higher on, an increased air velocity value is observed. The values are approximately 80% of the maximum velocity values for Fig. 5(b and c) while for the first case presented, the curve is smoother.

The temperature distribution of the half of the opening (without sun-shadings) open, in the y–z at the middle plane of the room and in the y–x plane is presented at $z=4.7$ m in Fig. 6. As it is observed near the chamber floor and the backward wall there is a small increase of the room temperature as was also measured and depicted through the experimental data.

## 4. Conclusions

This paper draws attention to the physical procedures governing air movement during the natural ventilation through the description of a computational method. The work demonstrates that numerical solutions for ventilation problems can be obtained quickly and economically. In the specific case of the single-sided ventilated buildings, the results have been presented and are not only physically plausible [14–18] but also in good agreement with available experiments. It is concluded that computational results are realistic and in good agreement with the experimental measurements, as presented in Table 3, and that computer simulations are now capable of assisting the designer to optimise ventilation in buildings. In addition they can dictate new designs from thermal comfort point of view.

## References

[1] S. Murakami, New scales for ventilation efficiency and their application based on numerical simulation of room airflow, in: Proceedings of International Symposium on Room Air Convection and Ventilation Effectiveness, University of Tokyo, 1992, pp. 22–38.

[2] M.W. Liddament, The role and application of ventilation effectiveness in design, in: Proceedings of International Symposium on Room Air Convection and Ventilation Effectiveness, University of Tokyo, 1992, pp. 59–75.

[3] A. Argiriou, Determination of the impact of shading devices in single-sided ventilation buildings, in: Proceedings of the Technical Report Presented at Contractors Meeting of the Project JOR3-CT96-00113, EU Report, 1997.

[4] S.V. Patankar, D.B. Spalding, A calculation procedure for heat, mass and momentum transfer in parabolic flows, Int. J. Heat Mass Trans. 21 (1972) 1565–1579.

[5] D.B. Spalding, Mathematical modelling of fluid mechanics, heat transfer and chemical-reaction processes, A Lecture Course, Imperial College, London, CFDU Report No. HT5/80/1, 1980.

[6] N.C. Markatos, D.B. Spalding, Computer simulation of fluid flow and heat/mass transfer phenomena — the PHOENICS code system, A Lecture Course, School of Mathematics, Thames Polytechnic, London, 1983.

[7] S.V. Patankar, Numerical Heat Transfer and Fluid Flow, Hemisphere Publishing Corporation, McGraw-Hill, New York, 1980.

[8] N.C. Markatos, G. Cox, Turbulent, buoyant heat transfer in enclosures containing a fire source, in: Proceedings of the 7th IHT Conference, Vol. 6, Hemisphere Publishing Corporation, 1982, pp. 373–379.

[9] N.C. Markatos, M.R. Malin, G. Cox, Mathematical modelling of buoyancy-induced smoke flow in enclosures, Int. J. Heat Mass Trans. 25 (1982) 63–75.

[10] W. Rodi, Turbulence Models and Their Application in Hydraulics — a State of the Art Review, University of Karlsruhe, SFB 80/T/127, 1980.

[11] N.C. Markatos, K.A. Pericleous, Laminar and turbulent natural convection in an enclosed cavity, Int. J. Heat Mass Trans. 27 (5) (1984) 755–772.

[12] D.B. Spalding, A general purpose computer program for multi-dimensional one or two-phase flow, Math. Comput. Simul. 13 (1981) 267.

[13] N.C. Markatos, T. Mukerjee, Three-dimensional computer analysis of flow and combustion in automotive internal combustion engines, J. Math. Comput. Simul. XIII (1981) 354–366.

[14] A. Schaelin, J. van der Maas, A. Moser, Simulation of airflow through large openings in buildings, ASHRAE Trans. Part 2 98 (1992).

[15] N.C. Markatos, Computer analysis of building ventilation and heating problems, in: Passive and Low Energy Architecture, Pergamon Press, Oxford, 1983, pp. 667–675.

[16] K.A. Papakonstantinou, C.T. Kiranoudis, N.C. Markatos, Mathema-tical modelling of environmental conditions inside historical build-ings, the case of the archaeological museum of Athens, Energy Building (1999), in press.

[17] K.A. Papakonstantinou, C.T. Kiranoudis, N.C. Markatos, Computa-tional analysis of thermal comfort, the case of the archaeological museum of Athens, Appl. Math. Model. (1999), in press.

[18] K.A. Papakonstantinou, C.T. Kiranoudis, N.C. Markatos, Numerical simulation of volatile organic compounds dispersion emitted from flooring materials in buildings, Drying Technol. (2000), in press.